

# N<sub>2</sub>O formation in the selective catalytic reduction of NO<sub>x</sub> with NH<sub>3</sub> at low temperature on CuO-supported monolithic catalysts

S. Suárez\*, J.A. Martín, M. Yates, P. Avila, J. Blanco

*Instituto de Catálisis y Petroleoquímica, C.S.I.C. C/Marie Curie 2, Campus de Cantoblanco, 28049 Madrid, Spain.*

Received 12 August 2004; revised 7 October 2004; accepted 9 October 2004

## Abstract

The formation of nitrous oxide in the selective catalytic reduction of NO<sub>x</sub> with ammonia was studied in nitric acid plant exhaust gas under low-temperature conditions. The important role played by the support in this process was evidenced by a comparison of CuO/γ-Al<sub>2</sub>O<sub>3</sub> and CuO/TiO<sub>2</sub> monolithic catalysts. Textural properties and CuO crystal phases were analysed. Temperature-programmed desorption of NH<sub>3</sub>, NO, and NO<sub>2</sub> and X-ray photoelectron spectroscopy (XPS) after in situ adsorption of NO and NO<sub>2</sub> experiments were carried out. Even at low temperature, N<sub>2</sub>O generation takes place at a greater rate for the catalysts supported on titania than for those on alumina. In the case of alumina, the N<sub>2</sub>O concentration detected was independent of the CuO content. For the CuO/TiO<sub>2</sub> system it was associated with the active phase configuration. After in situ adsorption of NO and NO<sub>2</sub>, a band associated with nitrate species was identified in the XPS spectra. Adsorbed NO<sub>3</sub><sup>-</sup> species seem to be responsible for the NO<sub>2</sub>, NO, and O<sub>2</sub> desorbed products detected in the NO<sub>x</sub>-TPD. The results suggests that NO<sub>3(ads)</sub><sup>-</sup> along with NH<sub>x(ads)</sub> species, were involved in N<sub>2</sub>O formation at low temperature.

© 2004 Elsevier Inc. All rights reserved.

**Keywords:** SCR; N<sub>2</sub>O formation; Low temperature; Monolithic catalyst; CuO/γ-Al<sub>2</sub>O<sub>3</sub>; CuO/TiO<sub>2</sub>; XPS in situ

## 1. Introduction

The selective catalytic reduction (SCR) of nitrogen oxides, with ammonia as a reductant, to produce nitrogen and water is one of the most widespread technologies for NO<sub>x</sub> abatement [1]. Nitric acid plant flue gas releases high concentrations of NO<sub>x</sub> into the atmosphere. The low temperature at which the effluent must be treated (180–250 °C), and the high concentration of NO<sub>2</sub> present in the flue gas (250–500 ppm) make this a singular case among NO<sub>x</sub> stationary sources.

Copper oxide-supported catalysts have shown excellent activity for NO<sub>x</sub> abatement with different reducing agents, such as CO [2], hydrocarbons [3], or ammonia. Recently, Blanco et al. have demonstrated the excellent performance of a CuO/NiO–Al<sub>2</sub>O<sub>3</sub> monolithic catalyst in the NO<sub>x</sub>

(NO:NO<sub>2</sub> = 1) reduction with ammonia at low temperature [4]. Wolberg and Roth identified three phases in CuO/Al<sub>2</sub>O<sub>3</sub> catalysts by X-ray adsorption edge spectroscopy: isolated Cu<sup>+2</sup>, copper aluminate surface phase, and crystalline CuO [5]. The effect of the NiO incorporation on the CuO/Al<sub>2</sub>O<sub>3</sub> system was studied by Knözinger et al. [6,7]; Ni<sup>+2</sup> tends to occupy the octahedral sites in subsurface layers and in the bulk. Thus, Ni<sup>+2</sup> leads to a Cu<sup>+2</sup> redistribution, with an enhanced segregation of copper on the surface. Previous studies carried out by Blanco et al. with CuO/Al<sub>2</sub>O<sub>3</sub> catalysts modified by the addition of small quantities of NiO have shown superior performance in NO<sub>x</sub> elimination from the tail gas in nitric acid plants [8,9].

The role of the support for the NO + NH<sub>3</sub> + O<sub>2</sub> reaction was analysed by Centi et al. [10], who studied copper oxide supported on Al<sub>2</sub>O<sub>3</sub>, TiO<sub>2</sub>, SiO<sub>2</sub>, and ZSM-5 catalysts; at 200 °C CuO/TiO<sub>2</sub> and CuO/ZSM-5 presented the highest conversion, whereas that based on Al<sub>2</sub>O<sub>3</sub> was the most active at temperatures above 350 °C.

\* Corresponding author. Fax: +34-91 585 47 60.  
E-mail address: [ssuarez@icp.csic.es](mailto:ssuarez@icp.csic.es) (S. Suárez).

Although many articles concerning  $\text{NO}_x$  abatement can be found in the literature, very few consider  $\text{N}_2\text{O}$  formation as a product of the SCR reaction [11–13], even though it is a strong greenhouse gas and contributes to the depletion of the stratospheric ozone layer. At present there is no legislation concerning  $\text{N}_2\text{O}$  concentration limits, although this is expected to change in the near future.

According to Odenbrand et al. [14], the three parameters that influence  $\text{N}_2\text{O}$  formation on  $\text{V}_2\text{O}_5/\text{TiO}_2\text{--SiO}_2$  catalysts are temperature, active phase content, and the presence of  $\text{H}_2\text{O}$  in the stream. An exponential relationship between temperature and  $\text{N}_2\text{O}$  formation on vanadium catalysts, reaching a selectivity for  $\text{N}_2\text{O}$  around 40% at 450 °C, was shown by Turco et al. [15]. Delahay et al. [16] observed a linear relationship between  $\text{N}_2\text{O}$  formation and  $\text{O}_2$  concentration in the feed.

The influence of the operating conditions on copper and vanadium oxide monolithic catalysts supported on alumina and titania, was analysed in a previous article [17]: high temperatures and  $[\text{NO}_x]/[\text{NO}]$  and  $[\text{NH}_3]/[\text{NO}_x]$  feed ratios promoted  $\text{N}_2\text{O}$  formation; a direct relationship between the presence of  $\text{NO}_2$  and  $\text{N}_2\text{O}$  production, studied by temperature-programmed surface reaction, was also reported.

This work is the third in a series of studies in which the formation of  $\text{N}_2\text{O}$  during the SCR reaction is analysed at low temperature [4,18]. Typical nitric acid SCR unit conditions were selected:  $[\text{NO}]/[\text{NO}_x] = 0.5$ ,  $[\text{NH}_3]/[\text{NO}_x]$  around 0.8 (to minimise the ammonia slip), and temperature  $T = 200^\circ\text{C}$ , similar to those studied in the previous articles. As the  $\text{N}_2\text{O}$  formation may be affected by mass transfer phenomena, it was considered convenient to carry out the study with catalysts in the same monolithic configuration as the ones used in the industrial SCR units. For this reason monolithic supports were prepared with the use of sepiolite, a natural magnesium silicate, as a binder [19,20].

The aim of this work was to analyse the role of the support and the metal oxide content in the  $\text{N}_2\text{O}$  formation in the SCR reaction at low temperature over  $\text{CuO}/\text{Al}_2\text{O}_3$  and  $\text{CuO}/\text{TiO}_2$  monolithic catalysts. Temperature-programmed desorption (TPD) experiments of  $\text{NH}_3$ ,  $\text{NO}$ , and  $\text{NO}_2$  and X-ray photoelectron spectroscopy (XPS) after in situ adsorption of  $\text{NO}$  and  $\text{NO}_2$  were carried out with these catalysts in order to relate the adsorbed species with  $\text{N}_2\text{O}$  production.

## 2. Experimental

### 2.1. Catalyst preparation

Two monolithic supports were manufactured by extrusion of doughs prepared by kneading boehmite (Condea) or anatase (Millenium) powders, with sepiolite (Tolsa S.A.) as a binder and water as described previously [4]. The  $\gamma\text{-Al}_2\text{O}_3$ :silicate and  $\text{TiO}_2$ :silicate ratios after heat treatment at 500 °C were 2/3 and 1/1 by weight, respectively. The monolithic

green bodies were subsequently dried and heat treated at 500 °C for 4 h in air to produce monolithic supports with the following geometric dimensions: square cell size 2.53 mm, wall thickness 0.89 mm, geometric surface  $8.6\text{ cm}^2\text{ cm}^{-3}$ , and cell density  $8.54\text{ cell cm}^{-2}$ .

Two series of catalysts were prepared by impregnation of titania and  $\gamma$ -alumina monolithic supports with aqueous solutions of copper and nickel nitrates (Panreac, purity  $\geq 99.9\text{ wt}\%$ ), while maintaining the  $[\text{CuO}]/[\text{NiO}]$  ratio at 10/1 (wt%). The role of nickel was to increase the dispersion of copper. After impregnation, the precursors were dried at room temperature for 24 h, and then at 100 °C for 12 h, and finally treated at 500 °C in air for 4 h.

### 2.2. Catalyst characterisation

*Copper content* was determined by inductively coupled plasma (ICP) optical emission spectroscopy of acid solutions of the ground catalysts in a Perkin–Elmer Optima 3300DV apparatus.

*Surface areas* were measured by nitrogen adsorption/desorption, with a Sorptomatic 1800. Samples were outgassed overnight at 250 °C to a vacuum of  $< 1 \times 10^{-2}\text{ Pa}$  to ensure a clean, dry surface. *The pore volumes* were determined by mercury intrusion porosimetry (MIP) with a CE Instruments Pascal 140/240 apparatus. By starting from vacuum and raising the pressure to 200 MPa, pore diameters from 150  $\mu\text{m}$  down to 7.5 nm can be determined. The Washburn equation is applied to transform the applied pressure into an equivalent diameter; the recommended values for the mercury contact angle and surface tension are  $141^\circ$  and  $484\text{ m Nm}^{-1}$ .

*X-ray diffraction (XRD)* patterns of ground samples of the monolithic catalysts were recorded on a Seifert 3000P powder diffractometer, with the use of  $\text{Cu-K}\alpha_1$  radiation ( $\lambda = 0.15406\text{ nm}$ ).

*X-ray photoelectron spectra* were acquired with a VG Escalab 200R spectrometer fitted with a monochromated  $\text{Mg-K}\alpha$  radiation ( $h\nu = 1253.6\text{ eV}$ ,  $1\text{ eV} = 1.6302 \times 10^{-19}\text{ J}$ ) 120-W X-ray source and a hemispherical electron analyser. The powdered samples were placed on a sample rod, introduced into a pretreatment chamber, and degassed at 25 °C and  $10^{-3}\text{ Pa}$  for 5 h prior to being transferred to the analysis chamber. Samples were treated in situ with  $\text{NO}$  or  $\text{NO}_2$  at 200 °C for 30 min in the pretreatment chamber. Residual pressure during data acquisition was maintained below  $3 \times 10^{-7}\text{ Pa}$ . The energy regions of the photoelectrons of interest ( $\text{Al } 2p_{3/2}$ ,  $\text{Ti } 2p_{3/2}$ ,  $\text{Si } 2p$ ,  $\text{Mg } 2p$ ,  $\text{Cu } 2p_{3/2}$ ,  $\text{N } 1s$ ) were scanned a number of times in order to obtain an acceptable signal-to-noise ratio. Accurate binding energies ( $\pm 0.2\text{ eV}$ ) were determined by referring to the  $\text{C } 1s$  peak at 284.9 eV.

*Temperature-programmed desorption* experiments of  $\text{NH}_3$ ,  $\text{NO}$ , and  $\text{NO}_2$  were carried out over the selected catalysts, which were placed in a stainless-steel micro-reactor, with an internal diameter of 1 cm and a length of 15 cm, operating at GHSV (NTP) = 20,700  $\text{h}^{-1}$  and  $P = 114\text{ kPa}$ . In order to fix the monolith of one cell in the centre of the

reactor, the space between the two bodies was filled with silicon carbide consisting of 0.84-mm particles. The connection between the mass spectrometer and the reactor was a steel capillary 1/16 inch in diameter heated to 200 °C to avoid condensation. The vacuum on the system was maintained at  $3 \times 10^{-4}$  Pa with a total sample flow for the measurement of  $10 \text{ mL min}^{-1}$ .

The gases at the micro-reactor inlet and the desorbed products were detected and quantified by mass spectrometry (Balzers Omnistar), with the use of a Channeltron detector. The following masses were evaluated:  $\text{N}_2$  (28), NO (30),  $\text{NO}_2$  (46),  $\text{O}_2$  (16),  $\text{N}_2\text{O}$  (44),  $\text{NH}_3$  (15,17). The measured ion currents were input to a solution matrix, and the individual concentrations of the components in the gas were determined via calibration factors. A Quantitative Analysis Module was used with a calibration factor library. For each component that is included in a calibration matrix, this library contains the calibration factors and the corresponding mass numbers, allowing the estimation of the overlap from different masses.

The catalysts were pretreated with oxygen (3 vol%) at 500 °C, with Ar as a gas balance. After cooling in argon to 180 °C, the gas ( $\text{NH}_3$ , NO, or  $\text{NO}_2$ ) was adsorbed until no signal variation of the gas was detected, and was subsequently purged with argon until no reactant was detected in the outlet. Finally, the temperature was increased at a rate of  $5 \text{ °C min}^{-1}$  from 180 to 500 °C.

### 2.3. Catalytic activity tests

Activity measurements of the monolithic catalysts were carried out in a continuous tubular glass reactor that operated at an integral regimen close to an isothermal axial profile. The reactor was 75 cm long and had an internal diameter of 2.54 cm. Ammonia was fed directly into the reactor bed to avoid the formation of ammonia salts [21]. Monoliths 20 cm long with nine cells were used; the gap between the catalyst and the reactor wall was filled with silicon carbide consisting of 0.84-mm particles.

The inlet and outlet NO and  $\text{NO}_2$  concentrations were determined by chemiluminescence with a Signal NO +  $\text{NO}_2$  analyser (Series 4000). Analysis of  $\text{N}_2\text{O}$  and  $\text{NH}_3$  was carried out by IR spectroscopy with a Signal 7000FT GFC Analyser and with an A.D.C. Double Beam Luft Type Infrared Gas Analyser, respectively. The evolution of the gas concentration at the reactor outlet was recorder by a Multichannel analogic-digital Register Yokowaga (Model 436006). The concentration data were acquired under steady-state conditions, after approximately 90 min of stabilization for each point.

The operating conditions for the experiments were as follows: gas hourly space velocity at normal conditions GHSV (NTP) =  $10,200 \text{ h}^{-1}$ , lineal velocity  $v_L = 0.98 \text{ m s}^{-1}$ , pressure  $P = 120 \text{ kPa}$ , temperature  $T = 200 \text{ °C}$ . The gas inlet compositions were  $[\text{NO}_x] = 1000 \text{ ppm}$ ,  $[\text{NO}]/[\text{NO}_x] =$

$0.54$ ,  $[\text{NH}_3]/[\text{NO}_x] = 0.77$ ,  $[\text{O}_2] = 4 \text{ vol\%}$ , and  $[\text{N}_2]$  to balance.

## 3. Results and discussion

### 3.1. Characteristics of the prepared catalysts

We prepared two series of  $\text{CuO}/\text{Al}_2\text{O}_3$  and  $\text{CuO}/\text{TiO}_2$  monolithic catalysts while varying the CuO/NiO content. The metal oxide content and textural and mechanical properties of the alumina and titania supported catalysts are listed in Tables 1 and 2, respectively. The number that appears in the label of each catalyst makes reference to the CuO content. The surface area of the supports was  $160 \text{ m}^2 \text{ g}^{-1}$  for the alumina and  $110 \text{ m}^2 \text{ g}^{-1}$  for the titania monoliths. As the active phase content increases, a slight decrease in the surface area and pore volume of the solids was observed, particularly for high-CuO/NiO content samples.

The ratio between the CuO content and the surface area was calculated by considering that copper was selectively impregnated on the alumina particles and not on the binder [4], and assuming a similar behaviour for the titania. The values obtained for this apparent surface density of CuO in the catalyst are listed in Tables 1 and 2 and expressed as micromoles of CuO per square meter of alumina ( $210 \text{ m}^2 \text{ g}^{-1}$ ) or titania ( $75 \text{ m}^2 \text{ g}^{-1}$ ), respectively.

### 3.2. Catalytic activity

The  $\text{NO}_x$  conversion and  $\text{NH}_3$  slip as a function of the CuO content for the  $\text{CuO}/\text{Al}_2\text{O}_3$  (AlCu) and  $\text{CuO}/\text{TiO}_2$  (TiCu) catalysts and  $\text{N}_2\text{O}$  produced during the SCR reaction at 200 °C are represented in Figs. 1a and 1b, respectively. For AlCu catalysts the  $\text{NO}_x$  conversion curves passed through a maximum that coincided with the minimum ammonia

Table 1  
Composition and textural properties of  $\text{CuO}/\gamma\text{-Al}_2\text{O}_3$  monolithic catalysts

Name	[CuO] (wt%)	[NiO] (wt%)	$S_{\text{BET}}$ ( $\text{m}^2 \text{ g}^{-1}$ )	Pore volume (MIP) ( $\text{cm}^3 \text{ g}^{-1}$ )	CuO surf. density ( $\mu\text{mol m}^{-2}$ ) (alumina)
AlCu-3	3.2	0.3	156	0.62	4.8
AlCu-5	4.8	0.5	156	0.62	7.2
AlCu-6	6.4	0.6	157	0.61	9.6
AlCu-8	8.1	0.8	156	0.56	12.1
AlCu-10	9.9	1.0	142	0.53	14.8

Table 2  
Composition and textural properties of  $\text{CuO}/\text{TiO}_2$  monolithic catalysts

Name	[CuO] (wt%)	[NiO] (wt%)	$S_{\text{BET}}$ ( $\text{m}^2 \text{ g}^{-1}$ )	Pore volume (MIP) ( $\text{cm}^3 \text{ g}^{-1}$ )	CuO surf. density ( $\mu\text{mol m}^{-2}$ ) (titania)
TiCu-1	1.4	0.1	108	0.71	4.7
TiCu-2	2.2	0.2	108	0.72	7.4
TiCu-4	4.0	0.4	104	0.69	13.4
TiCu-7	7.4	0.7	97	0.64	24.8

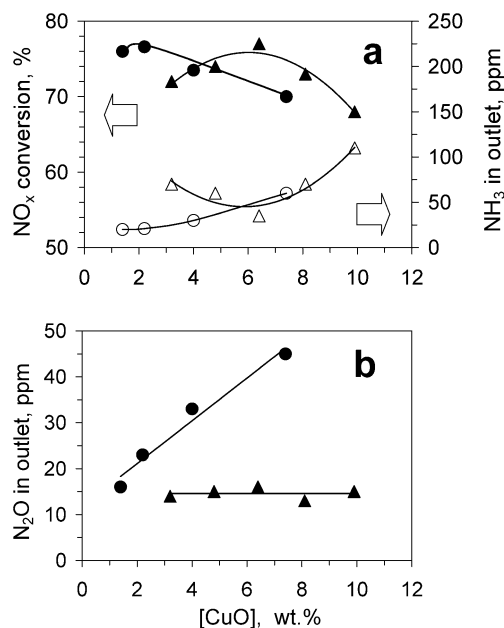


Fig. 1. (a) NO<sub>x</sub> conversion and NH<sub>3</sub> slip, and (b) N<sub>2</sub>O in the outlet as a function of the CuO content for (▲, △) CuO/γ-Al<sub>2</sub>O<sub>3</sub> and (●, ○) CuO/TiO<sub>2</sub> monolithic catalysts. Feed compositions: [NO<sub>x</sub>] = 1000 ppm, [NO]/[NO<sub>x</sub>] = 0.54, [NH<sub>3</sub>]/[NO<sub>x</sub>] = 0.77, [O<sub>2</sub>] = 4 vol%, [N<sub>2</sub>] = balance. Operating conditions: GHSV (NTP) = 10,200 h<sup>-1</sup>, *v*<sub>L</sub> = 0.98 Nm s<sup>-1</sup>, *T* = 200 °C, *P* = 120 kPa.

concentration at the outlet. The highest NO<sub>x</sub> conversion (ca. 75%) was close to that expected for the [NH<sub>3</sub>]/[NO<sub>x</sub>] ratio employed (maximum theoretical value of 77%). The major difference between the AlCu and TiCu curves was the copper oxide content at which this conversion was achieved: 2.2 wt% for the titania catalyst and 6.4 wt% for the alumina catalyst. For both series the SCR activity was lower at higher CuO contents.

Even at this low reaction temperature, N<sub>2</sub>O was detected at the outlet as a secondary product. In spite of the low N<sub>2</sub>O selectivity observed (lower than 10% in all cases), the two series of catalysts displayed significant differences with respect to their tendency towards N<sub>2</sub>O formation. For CuO/Al<sub>2</sub>O<sub>3</sub>, the selectivity remained practically constant; however, for CuO/TiO<sub>2</sub> a progressive increase in the N<sub>2</sub>O concentration with the CuO content was observed. These results indicated that the nature of the support and CuO oxide loading were key factors in the N<sub>2</sub>O selectivity.

In a previous study [18], the behaviour of these two catalysts for NH<sub>3</sub> oxidation reaction in the temperature range 180–450 °C was reported; the CuO/Al<sub>2</sub>O<sub>3</sub> catalyst (CuO = 6.4 wt%) was inactive at *T* = 200 °C, *P* = 120 kPa, and GHSV (NTP) = 15,000 h<sup>-1</sup>, with a feed composition of [NH<sub>3</sub>] = 1000 ppm and O<sub>2</sub> = 3 vol%. Nevertheless, the CuO/TiO<sub>2</sub> system ([CuO] = 2.2 wt%) displayed an ammonia conversion around 12% under similar conditions. Results in Fig. 1 show how the ammonia balance was satisfied for AlCu catalysts, whereas for TiCu the ammonia slip data corroborate the superior tendency of this system towards the NH<sub>3</sub> oxidation reaction, especially at high CuO loading. Al-

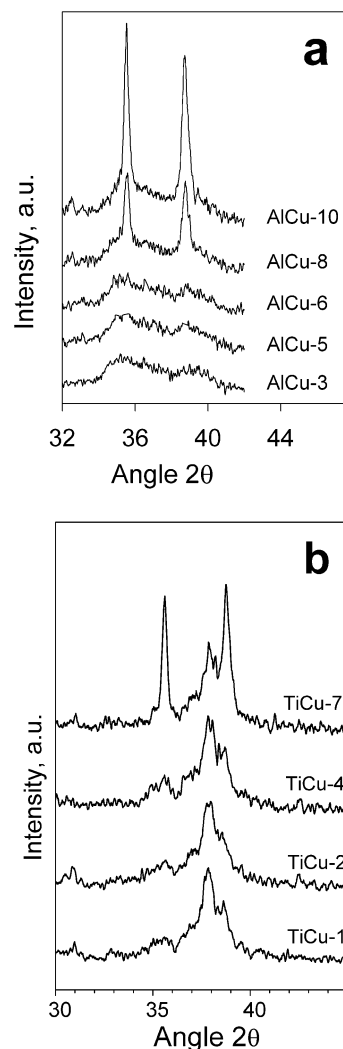


Fig. 2. X-ray diffraction patterns of (a) CuO/γ-Al<sub>2</sub>O<sub>3</sub> (b) CuO/TiO<sub>2</sub> catalyst with different CuO content in the range 2θ = 30°–40°.

though the N<sub>2</sub>O concentration detected in the outlet could arise from this reaction, the ammonia balance indicates that a different reaction path is involved, since to produce 1 mole of N<sub>2</sub>O, 2 moles of NH<sub>3</sub> are required.

### 3.3. X-ray diffraction analysis

The crystal phases formed in the AlCu and TiCu series studied by X-ray diffraction in the 2θ = 32°–40° range are shown in Fig. 2. The variation in the reflexion intensity at 36° and 39° for CuO/Al<sub>2</sub>O<sub>3</sub> catalysts with a CuO content lower than or equal to 6.4 wt% were ascribed to the alumina phase. At higher metal oxide concentrations two peaks centred at 2θ = 35.5° and 38.7° appeared. According to the ASTM 05-0661, these peaks were assigned to a CuO tenorite crystal phase [22–24]. The effect of Ni as a dispersive agent is obvious from a comparison of the concentration at which the CuO crystal phases started to appear with that previously reported by Friedman et al.

When the catalytic activity results (Fig. 1) and the XRD diffractograms of the samples (Fig. 2a) were correlated, a clear relationship between the  $\text{NO}_x$  conversion decrease with the appearance of a CuO crystal phase could be established. The values of CuO concentration at which the reduction in catalytic activity was observed corresponded to 8 wt% for the alumina and 4 wt% for the titania catalysts, AlCu-8 and TiCu-4, respectively. Similar values of copper surface density ( $12.1$  and  $13.4 \mu\text{mol CuO m}^{-2}$ , respectively) were obtained for the two samples (Tables 1 and 2). This result indicated how the surface area of the support affected the active phase dispersion and the formation of the copper oxide crystal phase.

With respect to the  $\text{N}_2\text{O}$  formation (Fig. 1b), a relation between the presence of a CuO crystal phase and  $\text{N}_2\text{O}$  formation could be assumed for TiCu. However, from the results obtained for AlCu systems, other parameters probably related to the nature of the support, or copper site density might also be involved.

### 3.4. Catalyst behaviour after $\text{NH}_3$ , $\text{NO}$ , and $\text{NO}_2$ adsorption

The species generated on the catalysts' surfaces were studied by TPD. The measurements were carried out with the AlCu-6 and TiCu-2 systems, since they displayed the highest catalytic activities (Fig. 1). The reactants  $\text{NH}_3$ ,  $\text{NO}$ , and  $\text{NO}_2$  (1000 ppm) were adsorbed at  $180^\circ\text{C}$  over an oxidised catalyst, with the use of an 8-cm-long monolith of one channel.

### 3.5. $\text{NH}_3$ : Temperature-programmed desorption

Temperature-programmed desorption curves recorded after  $\text{NH}_3$  adsorption over alumina and titania copper-supported catalysts are shown in Fig. 3a and 3b, respectively. At the starting temperature of  $180^\circ\text{C}$  and after the gas purge, only chemisorbed  $\text{NH}_3$  would remain on the catalyst surface. Broad ammonia desorption bands between  $180^\circ\text{C}$  and  $420^\circ\text{C}$ , with a maximum at  $250^\circ\text{C}$  characterised the desorption profiles of both catalysts. At higher temperatures  $\text{N}_2$ ,  $\text{NO}$ , and  $\text{H}_2\text{O}$  were desorbed.

These results indicated the presence of at least two types of acid sites where  $\text{NH}_3$  can be adsorbed. The first type, characterised by the  $\text{NH}_3$  desorption band centred at  $250^\circ\text{C}$ , was ascribed to Brønsted acid sites of the support. This band was also observed in the  $\text{NH}_3$  TPD of alumina, titania, or magnesium silicate without active phased incorporation [25].

The second type, responsible for the  $\text{N}_2$ ,  $\text{H}_2\text{O}$ , and  $\text{NO}$  desorption curves, was assigned to dissociatively adsorbed ammonia species such as  $\text{NH}_x$  ( $x = 0-2$ ) that could react with lattice oxygen to produce  $\text{N}_2$ ,  $\text{H}_2\text{O}$ , or even small quantities of  $\text{NO}$  (Fig. 3a). The  $\text{NH}_3$  TPD pattern of the supports (figure not included) showed no  $\text{N}_2$  desorption, which implied that the oxygen necessary to produce either  $\text{N}_2$  or  $\text{H}_2\text{O}$  was provided by the active phase [26]. The major difference

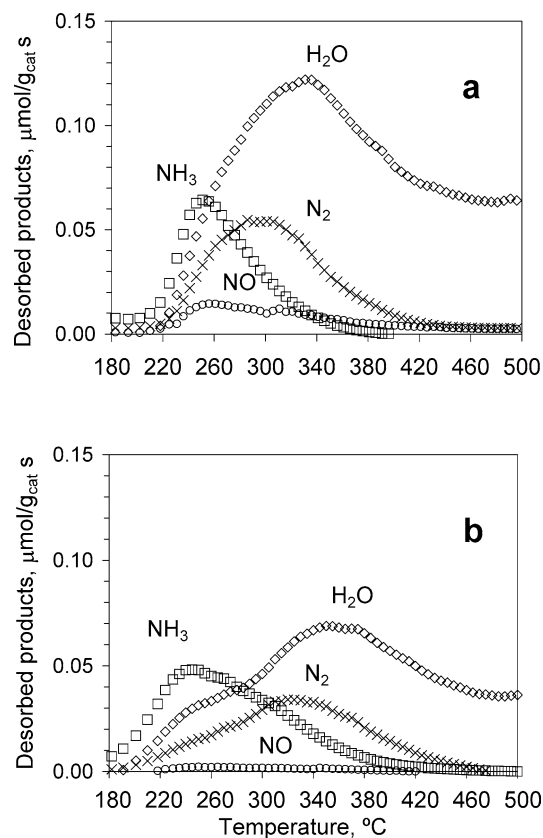


Fig. 3. Temperature-programmed desorption of  $\text{NH}_3$  after adsorption at  $180^\circ\text{C}$  for (a) AlCu-6 and (b) TiCu-2 monolithic catalysts. Desorption products: ( $\diamond$ )  $\text{H}_2\text{O}$ , ( $\square$ )  $\text{NH}_3$ , ( $\times$ )  $\text{N}_2$ , ( $\circ$ )  $\text{NO}$ . Feed composition:  $[\text{NH}_3] = 500$  ppm,  $[\text{Ar}] = \text{balance}$ . Desorption operating conditions: GHSV (NTP) =  $20,000 \text{ h}^{-1}$ ,  $v_L = 0.76 \text{ m s}^{-1}$ ,  $[\text{Ar}] = 100 \text{ vol\%}$  and  $T = 180-500^\circ\text{C}$  at a rate of  $5^\circ\text{C min}^{-1}$ .

between the  $\text{N}_2$  desorption profiles of the two catalysts is the initial temperature at which  $\text{N}_2$  started to desorb. Even at a temperature as low as  $180^\circ\text{C}$ , TiCu-2 produced nitrogen, indicating that  $\text{NH}_{x(\text{ads})}$  species generated on the titania catalyst are more active than those produced over the alumina system.

The total amount of desorbed  $\text{N}_2$ ,  $\text{H}_2\text{O}$ ,  $\text{NH}_3$ , and  $\text{NO}$  was calculated by integration of the areas under the curves in the temperature range between  $180^\circ\text{C}$  and  $500^\circ\text{C}$  (Table 3).  $\text{N}_2$  and  $\text{NO}$  are selectively produced by oxidised copper species (dispersed or aggregated) according to the equations



From the TPD experiments and considering the reaction stoichiometry of Equations (1) and (2), we evaluated the  $\text{Cu}^{+2}$  species accessible to react with ammonia [26]. The results obtained (Table 3) point out that although metal oxide content on the AlCu-6 catalyst (6.4 wt%) was three times larger than that over TiCu-2 (2.2 wt%), the copper species accessible in the latter was higher (93 vs 73%), thus explaining the similar performance towards  $\text{NO}_x$  conversion displayed by the two systems (Fig. 1a).

### 3.6. NO and NO<sub>2</sub>: Temperature-programmed desorption

TPD experiments were carried out in order to determine the adsorption capacity of the catalysts towards NO and NO<sub>2</sub>. Experiments were conducted with the procedure as used for NH<sub>3</sub> TPD. The product desorption curves after NO or NO<sub>2</sub> adsorption for AlCu-6 and TiCu-2 and those for the corresponding supports are shown in Figs. 4 and 5, respectively.

The supports and catalysts displayed a NO desorption curve with two bands centred at different temperatures. Bands were assigned according to the shape of

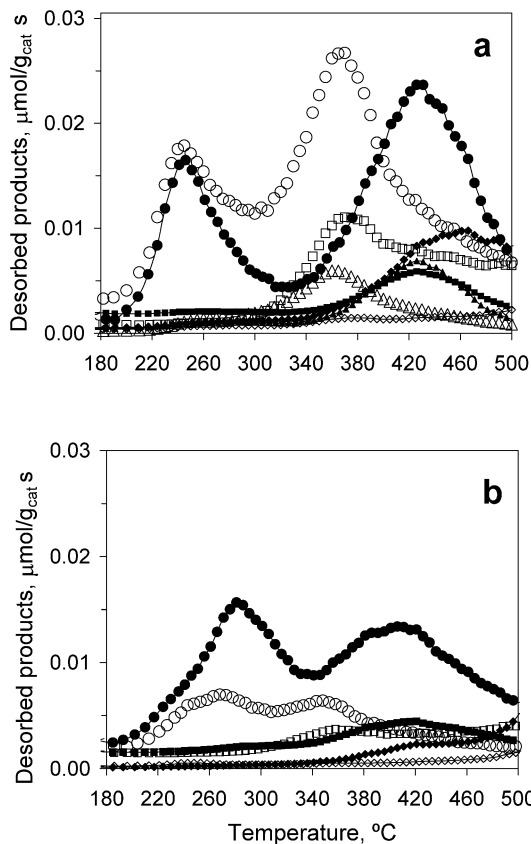


Fig. 4. Temperature-programmed desorption of NO after adsorption at 180 °C for supports (filled) and catalysts (empty). (a) AlCu-6 and alumina support, (b) TiCu-2 and titania support. Desorption products: (■, □) O<sub>2</sub>, (▲, △) NO<sub>2</sub>, (●, ○) NO, (◆, ◇) N<sub>2</sub>O. Feed composition: [NO] = 1000 ppm, [Ar] = balance. Desorption operating conditions: GHSV (NTP) = 20,000 h<sup>-1</sup>,  $v_L = 0.76 \text{ m s}^{-1}$ , [Ar] = 100 vol% and  $T = 180\text{--}500^\circ\text{C}$  at a rate of  $5^\circ\text{C min}^{-1}$ .

the NO TPD curves (not shown) obtained for raw alumina, titania, and magnesium silicate materials treated at 500 °C. The results obtained in these previous experiments showed that the magnesium silicate presents a NO desorption band centred at 250 °C, and the alumina or titania desorbed the NO together with N<sub>2</sub>O, NO<sub>2</sub>, and O<sub>2</sub> around 420 °C and 380 °C, respectively. Thus, in Fig. 4a the first band centred at 245 °C, observed for both Al/Sep and AlCu-6, was assigned to the silicate NO adsorption sites. This band remained unaltered when the active phase was added to the support, indicating that the NO adsorption sites over the magnesium silicate remained unchanged.

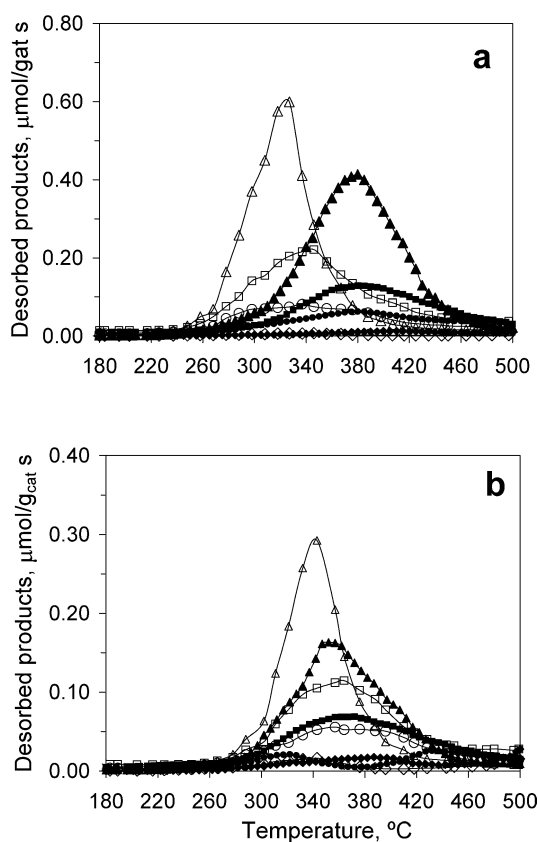


Fig. 5. Temperature-programmed desorption of NO<sub>2</sub> after adsorption at 180 °C for supports (filled) and catalysts (empty). (a) AlCu-6 and alumina support (b) TiCu-2 and titania support. Desorption products: (▲, △) NO<sub>2</sub>, (■, □) O<sub>2</sub>, and (●, ○) NO. Feed composition: [NO<sub>2</sub>] = 1000 ppm, [Ar] = balance. Desorption operating conditions: GHSV (NTP) = 20,000 h<sup>-1</sup>,  $v_L = 0.76 \text{ m s}^{-1}$ , [Ar] = 100 vol% and  $T = 180\text{--}500^\circ\text{C}$  at a rate of  $5^\circ\text{C min}^{-1}$ .

Table 3

TPD results from 180–500 °C after ammonia adsorption at 180 °C

Name	NH <sub>3</sub> (μmol g <sup>-1</sup> )	N <sub>2</sub> (μmol g <sup>-1</sup> )	H <sub>2</sub> O (μmol g <sup>-1</sup> )	NO (μmol g <sup>-1</sup> )	NH <sub>3(ads)</sub> dissociatively (μmol g <sup>-1</sup> )	CuO accessible (%)
Al/Sep	135	–	–	–	–	–
AlCu-6	57	78	274	21	177	73
Ti/Sep	91	–	–	–	–	–
TiCu-2	51	43	121	–	86	93

Table 4  
Desorbed products after NO or NO<sub>2</sub> adsorption at 180 °C

Gas adsorbed	Catalyst	NO (μmol g <sup>-1</sup> )	NO <sub>2</sub> (μmol g <sup>-1</sup> )	O <sub>2</sub> (μmol g <sup>-1</sup> )	N <sub>2</sub> O (μmol g <sup>-1</sup> )
NO	AlCu-6	50	5	17	2
	Al/Sep	41	9	10	10
	TiCu-2	17	1	10	2
	Ti/Sep	38	7	11	6
NO <sub>2</sub>	AlCu-6	76	239	165	5
	Al/Sep	61	231	130	11
	TiCu-2	47	102	83	13
	Ti/Sep	23	92	61	18

The second NO desorption band observed at higher temperature (425 °C) for the Al/Sep system and associated with different nitrogen oxides and oxygen was characteristic of Al<sub>2</sub>O<sub>3</sub>. Copper and nickel oxide incorporation on alumina/silicate system causes a decrease in the desorption temperature to 360 °C and produced a relative increase in the oxygen desorbed fraction. The bond strength of the NO in the catalyst was modified because the sites of NO adsorption on the alumina were altered by the metal oxides or because aluminium sites were blocked by copper/nickel sites. The desorption profiles at high temperature show that the support presented a higher tendency to produce N<sub>2</sub>O, which was drastically reduced by incorporation of the metal oxides.

In Fig. 4b the results obtained for the TiCu-2 system and the Ti/Sep support are shown. The curves display a behaviour similar to that found for the alumina system. The band corresponding to the magnesium silicate was also observed at low temperature, and the band centred around 400 °C was attributed to the NO adsorption of the titania surface. In this case, when the active phase was incorporated over the Ti/Sep there was a large decrease in the band intensities, along with a shift to lower temperatures, indicating a reduction in the number of NO adsorption sites and a weakening of their strength. That the reactivity of the NO adsorbed species on the catalyst based on TiO<sub>2</sub> was higher than the reactivity of the species on the catalyst based on Al<sub>2</sub>O<sub>3</sub> was clear from a consideration of the shift of the high temperature band. In the former the peak appeared at 345 °C, whereas in the latter the band was centred at 365 °C. Moreover, the results show that the magnesium silicate NO adsorption sites were also modified by the addition of CuO/NiO, suggesting that the active phase impregnation process was not selective for TiO<sub>2</sub>, and there was a partial deposition of the metal oxide in the silicate.

The quantities of desorbed NO, NO<sub>2</sub>, O<sub>2</sub>, and N<sub>2</sub>O for supports and CuO/NiO catalysts are summarised in Table 4. The capacity of these systems to adsorb NO (Figs. 4a and 4b) was significantly lower than their capacity to adsorb ammonia. The NO adsorption studies carried out on previously oxidised CuO/Al<sub>2</sub>O<sub>3</sub> catalyst by Knözinger et al. [27] displayed two desorption bands centred at 220 °C and 400 °C, respectively. Taking into account the FTIR spectra, the au-

thors assigned the high temperature band to the transformation of Cu<sup>+</sup>-ONO<sup>-</sup> into Cu<sup>+</sup>-ONO<sub>2</sub><sup>-</sup> species. At high temperatures the nitrate complex is decomposed into NO and O<sub>2</sub>, reducing the Cu<sup>+</sup> to Cu<sup>0</sup>. Centi et al. [32,33] also identified nitrates species adsorbed to copper catalysts.

Considering the results obtained in this work for catalysts and supports, it could be suggested that nitrate species M<sup>n+</sup>-(O-NO<sub>2</sub>)<sup>-</sup>, where M is Cu, Ni, Al, or even Ti, could be responsible for the NO and O<sub>2</sub> desorption bands observed in the NO TPD, according to Eq. (3)

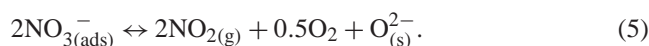


Nevertheless, in order to explain the formation of N<sub>2</sub>O and that of NO<sub>2</sub> in the supports, other reactions should be considered. One possibility is the NO autoxido-reduction reaction yielding NO<sub>2</sub> + N<sub>2</sub>O, as shown in Eq. (4). According to this reaction the [NO<sub>2</sub>]/[N<sub>2</sub>O] ratio is 1, which is consistent with the data reported in Table 4.



The product desorption curves for AlCu-6 and TiCu-2 catalysts after NO<sub>2</sub> adsorption are displayed in Fig. 5, together with those for the supports. The systems show a higher adsorption capacity for NO<sub>2</sub> than for NO, particularly the alumina supported catalysts. Along with the NO<sub>2</sub> band, N<sub>2</sub>O, NO, and O<sub>2</sub> were also observed. Although the N<sub>2</sub>O band seems to be negligible (because of the graph scale), the data quoted in Table 4 clearly indicate that N<sub>2</sub>O was also produced, and it is especially promoted over TiO<sub>2</sub> systems. The reaction described in Eq. (4) could explain this nitrous oxide formation.

Copper/nickel oxide incorporation led to a greater quantity of desorbed NO<sub>2</sub> and a decrease in the desorption band temperature. As discussed above for NO TPD, NO<sub>3(ads)</sub><sup>-</sup> species could justify the NO and O<sub>2</sub> desorption in an equimolecular ratio. However, an excess oxygen concentration was observed in all systems, indicating that other reactions that involve oxygen production are taking place. Apostolescu et al. [28] have recently studied the adsorption of NO<sub>2</sub> over alumina by thermal decomposition of the species formed. They suggested that this process takes place via formation of nitrite species, which are subsequently oxidized by NO<sub>2</sub> to yield NO<sub>3</sub><sup>-</sup> and gaseous NO. Thermal treatment leads to decomposition of nitrate species in the high temperature region. The latter reaction results in the formation of NO<sub>2(g)</sub> and O<sub>2(gas)</sub> in the molar ratio of 4 and the reformation of the Al<sub>2</sub>O<sub>3</sub> surface, according to the following reaction:



However, the experimental data given in Table 4 show a NO<sub>2</sub>/O<sub>2</sub> ratio of only about 1.5. The complex mechanism that takes place in these systems seems to indicate that the nitrate decomposition to NO and O<sub>2</sub> (Eq. (3)) and its decomposition to NO<sub>2</sub> and O<sub>2</sub> (Eq. (5)) may occur simultaneously.

Thus, considering the oxygen desorbed as a sum of the two contributions, a good fit may be obtained.

### 3.7. X-ray photoelectron spectroscopy results

In order to determine the nature of the  $N_xO_y$  adsorbed species, XPS experiments were carried out over the selected catalysts. Fresh samples and samples subjected to in situ adsorption of NO and  $NO_2$  were studied. The N 1s, in addition to Cu  $2p_{3/2}$ , Si 2p, Mg 2p, Al  $2p_{3/2}$ , or Ti  $2p_{3/2}$  core levels, were measured for TiCu-2 and AlCu-6 samples. The XPS binding energy (BE) values for copper and nitrogen and the N/Si, N/Cu surface atomic ratio are compiled in Table 5. All values are related to the C 1s binding energy of 284.1 eV.

The main XPS feature of the CuAl-6 sample was the appearance of spin-orbit split Cu  $2p_{1/2}$ , and  $2p_{3/2}$ , along with their shake-up satellite, indicating the characteristic peaks of  $Cu^{+2}$ . The spectra reveal that copper species are in an oxidation state of  $Cu^{2+}$ , attributed to the large peak with a maximum around 934.5 eV and the satellite peak at a binding energy around 10 eV higher [7,23]. The ratio between these two peaks was about 2. The presence of reduced species was ruled out, because of the oxidant conditions used in the catalyst treatment. Furthermore, the intensity of the satellite peak did not show any modification with the gas pretreatment.

The  $Cu^{+2}$  main peak presented a shift to a higher binding energy (934.5 eV) with respect to the theoretical peak corresponding to CuO (933.5 eV). According to Friedman and Freeman [23], this is due to the formation of a  $CuAl_2O_4$  spinel phase. Moreover, the deconvolution of this peak indicates two contributions, one centred at 933.6 eV and the other at 934.5 eV. Thus, the presence of both CuO and  $CuAl_2O_4$  spinel phases defines the catalyst structure.

For CuTi the same general trend was observed. Two  $Cu^{+2}$  phases were detected in the XPS analysis. The deconvolution of the Cu  $2p_{3/2}$  peaks centred at 934.5 eV indicated the presence of a CuO phase (933.0 eV), and that at 935 eV corresponded to a Cu–O–Ti phase, as previously described for CuO/TiO<sub>2</sub> catalysts by Cordoba et al. [29].

After NO or  $NO_2$  treatment, a chemical shift of 0.8 eV towards higher binding energy was observed, suggesting that  $N_xO_y$  species, strongly adsorbed to cupric ions, modified the density of the electronic cloud, producing a variation in the charge distribution of the complex. In the case of TiCu-2 the shift was observed only after  $NO_2$  adsorption.

In all cases, the intensity of the  $Cu^{+2}$  main peak for TiCu was higher than the intensity of the peaks for Cu–Al. This may be indicative of the higher dispersion of copper species in the former (corroborating the data obtained by  $NH_3$  TPD) or symptomatic of the higher porosity of the alumina support, where copper species may be located inside the mesopores, where they would be inaccessible to the XPS technique.

The N 1s spectra are represented in Fig. 6. The spectra are characterized at least by two bands, centred around 400 and 407 eV. The former peak may be assigned to  $N_2O$  or NO adsorbed species, whereas the latter coincides with that of the  $NaNO_3$  spectra, suggesting that  $NO_3^-$  species may be generated in the adsorption process [30]. The existence of these bands even in the fresh samples has been attributed to  $N_xO_y$  remainders from the copper and nickel nitrate salts used for catalyst preparation. With increasing oxidative power of the adsorbed molecule, the bands at lower binding energy disappear, becoming more important those centred at higher BE. These observations are reflected in the contribution of each band to the total area under the curves (Table 5). The N/Si atomic ratio increased according to the series: no pretreatment < NO <  $NO_2$ . The results suggest that strongly adsorbed  $NO_3^-$  species are generated on the catalyst surface after exposure to nitrogen oxide, especially  $NO_2$ . The NO and  $NO_2$  pretreatment produces a shift of the band at 407 eV with respect to the fresh sample. This effect is in accordance with the shift detected in  $Cu^{+2}$  spectra (Table 5) and corroborates the idea that soft electronic effects produced by nitrate species adsorbed on  $Cu^{+2}$  sites may shift the electronic cloud towards the nitrate species, generating a  $NO_3^-$  ( $\delta^-$ ) and  $Cu^{+2}$  ( $\delta^+$ ).

The influence of the support is reflected when the N/Cu atomic ratios of the two catalysts are compared. The N/Cu

Table 5  
Binding energies of core electrons, and N/Si surface atomic ratio, for the fresh sample, and after adsorption of NO,  $NO_2$ , at 200 °C

Pre-treatment	Cu $2p_{3/2}$	Cu $2p_{3/2}$ satellite	N 1s	N/Si	N/Cu
(a) AlCu-6 fresh catalyst	934.5	943.5	399.3 (60) 407.9 (38)	–	–
NO	935.3	943.4	399.2 (33) 407.1 (67)	0.031	0.32
$NO_2$	935.5	943.4	400.4 (14) 407.2 (86)	0.051	0.43
(b) TiCu-2 fresh catalyst	934.5	943.1	399.8 (61) 407.7 (39)	0.041	0.42
NO	934.5	943.0	400.1 (26) 406.8 (74)	0.051	0.52
$NO_2$	935.3	943.6	399.9 (25) 406.9 (75)	0.098	0.99

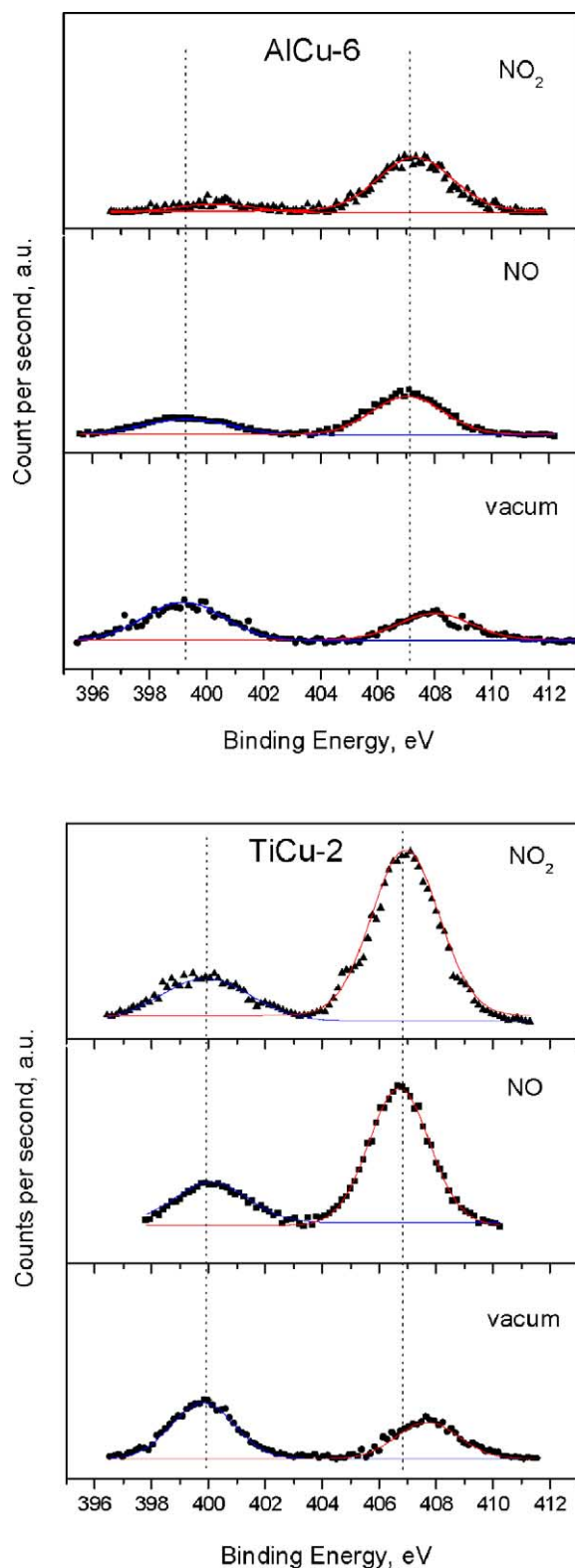


Fig. 6. N 1s core level spectra for fresh samples and after adsorption of NO, and NO<sub>2</sub> at 200 °C.

atomic ratios are higher over the titania-based catalysts than for the alumina-based catalysts. These observations are in good agreement with the NO<sub>2</sub> TPD results, where the NO<sub>2</sub>, NO, and O<sub>2</sub> desorbed bands of TiCu-2 were less intense and

appear at relatively higher temperatures than those corresponding to the AlCu-6 catalyst.

Based on the results obtained by XPS after SCR reaction in the presence of NO<sub>2</sub> catalyst, Blanco et al. proposed a Langmuir–Hinshelwood mechanism for CuO/Al<sub>2</sub>O<sub>3</sub> [31]. In the studied system, copper remains as the Cu<sup>+</sup> species under steady-state conditions, and these species are more easily reoxidised by NO<sub>2</sub> than they are by O<sub>2</sub> or NO. The proposed mechanism involved dissociatively adsorbed ammonia on Cu<sup>+2</sup>-forming NH<sub>2</sub> species and a reduced site. Nitrogen dioxide can be transformed to NO according to the process Cu<sub>2</sub>O + NO<sub>2</sub> → 2Cu + NO<sub>(ads)</sub>, leading to a high concentration of NO adsorbed to the surface. Centi et al. [32,33], who analysed the behaviour of CuO catalysts supported on Al<sub>2</sub>O<sub>3</sub> and ZSM-5 by ESR, UV–vis, etc., proposed the formation of ammonium nitrates species, generated by the transformation of nitrites to nitrates in CuO and in the presence of O<sub>2</sub> and NH<sub>x(ads)</sub>, as intermediates to N<sub>2</sub>O formation. For CuO/ZSM-5 samples, Mizumoto et al. [34,35] suggested that N<sub>2</sub>O formation is related to the SCR reaction and to reduced copper sites. For Pt/Al<sub>2</sub>O<sub>3</sub> Yamaguchi et al. [36] proposed that NH<sub>(ads)</sub> species, along with NO or reduced sites, are responsible for N<sub>2</sub>O formation. Otto et al. [37] pointed out that reduced sites generated by the dissociative NH<sub>3</sub> adsorption reacted with two NO molecules to produce N<sub>2</sub>O. Meier and Gut [38] put forward the reaction between NO and NH<sub>3</sub> as responsible for the N<sub>2</sub>O formation. In the NO/NO<sub>2</sub> TPD experiment carried out in this work, the N<sub>2</sub>O desorption was negligible and occurred at a higher temperature than the SCR reaction. Thus it may be assumed that the N<sub>2</sub>O does not come from the NO or NO<sub>2</sub> alone. But the oxidation state of the catalyst was different under a NO<sub>x</sub> or SCR atmosphere, where ammonia was also present. In fact, Mizumoto and Otto et al. suggested that reduced sites may be involved in the N<sub>2</sub>O formation.

The results obtained in this work point out the important role of the support in the formation of N<sub>2</sub>O as a secondary product during the SCR reaction. For alumina samples, the N<sub>2</sub>O concentration detected in the reactor outlet was independent of the CuO/NiO loading. The ammonia oxidation reaction or even the reaction between NO<sub>x</sub> and NH<sub>3</sub> were excluded as a possible way to produce N<sub>2</sub>O. In fact, when the NO<sub>x</sub> conversion started to decrease, no appreciable influence of the N<sub>2</sub>O amount was observed. Over catalysts supported on titania, a progressive increase in the N<sub>2</sub>O formation with the metal loading was observed, suggesting that properties related to active phase configuration are involved in the N<sub>2</sub>O formation process. The NO<sub>3(ads)</sub><sup>-</sup> adsorbed species generated in the presence of a NO/NO<sub>2</sub> gas mixture observed by XPS and responsible for the NO<sub>2</sub>, NO, and O<sub>2</sub> desorption of the NO/NO<sub>2</sub> TPD could react with NH<sub>x</sub> species (and was more reactive in the case of CuTi catalysts) to produce N<sub>2</sub>O, according to the mechanism proposed by Centi et al.

#### 4. Conclusions

The influence of the support and CuO/NiO content in the N<sub>2</sub>O formation during the SCR reaction at low temperature was studied. For this purpose CuO–NiO/TiO<sub>2</sub> and CuO–NiO/ $\gamma$ -Al<sub>2</sub>O<sub>3</sub> monolithic catalysts were analysed, with the use of magnesium silicate as a binder. N<sub>2</sub>O formation is a complex process in which different intermediates may be involved, especially when supports of several components are used. The studied supports had a tendency towards N<sub>2</sub>O formation in the presence of NO/NO<sub>2</sub>, and this ability is strongly affected by deposition of the active phase. The catalytic activity results indicate that the ammonia oxidation reaction was not the main path for the N<sub>2</sub>O formation, even at high metal oxide loading under the selected operating conditions. The existence of NO<sub>3</sub><sup>–</sup><sub>(ads)</sub> species in the catalyst after adsorption of NO or NO<sub>2</sub> was demonstrated by NO or NO<sub>2</sub> TPD and XPS. The presence of dissociatively adsorbed ammonia responsible for the nitrogen formation observed by NH<sub>3</sub> TPD is related to NH<sub>x</sub> adsorbed species. Thus, the reaction between these NO<sub>3</sub><sup>–</sup><sub>(ads)</sub> and NH<sub>x</sub>(ads) species adsorbed on Cu<sup>2+</sup>, and especially reactive on the CuTi system, is suggested as a feasible path for producing N<sub>2</sub>O.

#### Acknowledgments

The authors gratefully acknowledge the CICYT (projects MAT 2001-1597 y MAT 2000-0080-P4-02) and the Ministry for Science and Technology (Spain) (I3P program) for financial support and Prof. J.L.G. Fierro for the XPS measurements and his valuable contribution to the XPS spectra interpretation.

#### References

- [1] H. Bosch, F. Janssen, *Catal. Today* 2 (1988) 369.
- [2] T.J. Huang, T.-C. Yu, *Appl. Catal.* 71 (1991) 275.
- [3] H. Hamada, Y. Kintaichi, M. Sasaki, T. Ito, M. Tabata, *Appl. Catal.* 75 (1991) L1.
- [4] J. Blanco, P. Avila, S. Suarez, M. Yates, J.A. Martín, L. Marzo, C. Knapp, *Chem. Eng. J.* 97 (2004) 1.
- [5] A. Wolberg, J.F. Roth, *J. Catal.* 15 (1969) 250.
- [6] R. Hierl, H. Knözinger, N. Thiele, *J. Catal.* 69 (1981) 475.
- [7] G. Ertl, R. Hierl, H. Knözinger, N. Thiele, H.P. Urbach, *Appl. Surf. Sci.* 5 (1980) 49.
- [8] J. Blanco, J.F. García de la Banda, P. Avila, F. Melo, *J. Phys. Chem.* 90 (1989) 4789.
- [9] J. Blanco, P. Avila, L. Marzo, *Catal. Today* 17 (1993) 325.
- [10] G. Centi, C. Nigro, S. Perathoner, G. Stella, *Catal. Today* 17 (1993) 159.
- [11] T. Salvese, S. Roesch, P.A. Sermon, P. Kaur, *Top. Catal.* 16 (1–4) (2001) 381.
- [12] E. Joubert, J.C. Menezes, D. Duprez, J. Barbier, *Top. Catal.* 16 (1–4) (2001) 225.
- [13] P. Ciambelli, P. Corbo, F. Migliardini, *Catal Today* 59 (3–4) (2000) 279.
- [14] C.U.I. Odenbrand, P.L.T. Gabrielson, J.G.M. Brandin, L.A.H. Andersson, *Appl. Catal.* 78 (1991) 109.
- [15] G. Bagnasco, G. Busca, P. Galli, M.A. Massucci, K. Melanová, P. Patrono, G. Ramis, M. Turco, *Appl. Catal. B* 28 (2000) 135.
- [16] G. Delahay, B. Coq, S. Kieger, B. Neveu, *Catal. Today* 54 (1999) 431.
- [17] J. Blanco, P. Avila, S. Suárez, J.A. Martín, C. Knapp, *Appl. Catal. B* 28 (2000) 235.
- [18] S. Suárez, S.M. Jung, P. Avila, P. Grange, J. Blanco, *Catal. Today* 75 (2002) 331.
- [19] P. Avila, J. Blanco, A. Bahamonde, J.M. Palacios, C. Barthelemy, *J. Mater. Sci.* 28 (1993) 4113.
- [20] J. Blanco, M. Yates, P. Avila, A. Bahamonde, *J. Mater. Sci.* 29 (1994) 5927.
- [21] J. Blanco, P. Avila, C. Barthelemy, A. Bahamonde, J.A. Odriozola, J.F. Garcia de la Banda, *Appl. Catal.* 55 (1989) 151.
- [22] A. Wolberg, J.L. Ogielvie, J.F. Roth, *J. Catal.* 19 (1970) 86.
- [23] R.M. Friedman, J.J. Freeman, F.W. Lytle, *J. Catal.* 55 (1978) 10.
- [24] J.J. Freeman, R.M. Friedman, *J. Chem. Soc. Faraday Trans.* 1–74 (1978) 758.
- [25] S. Suárez, Desarrollo de catalizadores SCR altamente selectivos a nitrógeno para plantas de ácido nítrico Ph.D. Thesis, Madrid (2002).
- [26] J.M. Rodríguez Blas, Desarrollo de catalizadores monolíticos basados en CuO/NiO para la eliminación de NO<sub>x</sub>, Ph.D. Thesis, Madrid (1997).
- [27] R. Hierl, H.-P. Urbach, H. Knözinger, *J. Chem. Faraday Trans.* 88 (3) (1992) 355.
- [28] N. Apostolescu, T. Schröder, S. Kureti, *Appl. Catal. B: Env.* 51 (2004) 43.
- [29] G. Córdoba, M. Viniegra, J.L.G. Fierro, J. Padilla, R. Arrollo, *J. Solid State Chem.* 138 (1998) 1.
- [30] C.D. Wagner, W.M. Riggs, L.E. Davis, J.F. Moulder, in: G.E. Muilenbag (Ed.), *Handbook of X-ray photoelectron spectra*, Perkin–Elmer Corporation, Eden Prairie, MN, 1979.
- [31] J. Blanco, P. Avila, J.L.G. Fierro, *Appl. Catal. A* 96 (1993) 331.
- [32] G. Centi, S. Perathoner, P. Bigliano, E. Giamello, *J. Catal.* 151 (1995) 75.
- [33] G. Centi, S. Perathoner, *J. Catal.* 152 (1995) 93.
- [34] M. Mizumoto, M. Yamazoe, T. Seiyama, *J. Catal.* 55 (1978) 119.
- [35] M. Mizumoto, M. Yamazoe, T. Seiyama, *J. Catal.* 59 (1979) 3109.
- [36] M. Yamaguchi, K. Matsushita, K. Takami, *Hyd. Proc.* 55 (8) (1976) 101.
- [37] K. Otto, M. Shelef, J.T. Kummer, *J. Phys. Chem.* 74 (13) (1970) 2690.
- [38] H. Meier, G. Gut, *Chem. Eng. Sci.* 33 (1978) 123.